Analysis of 5−10 GHz Higher-Order Lamb Acoustic Waves in Thin-Film Scandium Aluminum Nitride

Sinwoo Cho†, Jack Guida‡, Jack Kramer†, Omar A. Barrera†, Vakhtang Chulukhadze†, Can Cui†, Siddhartha Ghosh‡, and Ruochen Lu†
†Department of Electrical and Computer Engineering, The University of Texas at Austin, Austin, US
‡Department of Electrical and Computer Engineering, Northeastern University, Boston, US
sinwoocho@utexas.edu

***Summary*— In this work, we report a systematic analysis of acoustic waves in thin-film 30% scandium-doped aluminum nitride (ScAlN) between 5 and 10 GHz. Higher-order Lamb mode acoustic delay line (ADL) testbeds are implemented in ScAlN, surpassing the operation frequency of prior reported works. Transducers with different lateral wavelengths (λ) between 0.8 µm and 1.4 µm are fabricated in 500 nm thick sputtered ScAlN thin films. Key propagation characteristics, e.g., group velocity (v_g) and acoustic propagation quality factor (Q), are experimentally studied for the first time for Lamé and first-order symmetric (S1) modes beyond 6 GHz. This work presents an approach to extract the intrinsic acoustic loss in piezoelectric thin films, guiding future frequency scaling of microacoustic devices into mm-wave bands.**

Keywords*— *Acoustic delay line, Lamé mode, Lamb wave, piezoelectric devices, thin-film devices, scandium aluminum nitride

I. Introduction

Radio frequency (RF) acoustic devices are indispensable signal-processing components for mobile communications. Acoustic devices have two key advantages over electromagnetic (EM) counterparts, namely much shorter wavelengths by several orders of magnitude, and lower attenuation at radio frequency (RF) [1]. Aluminum nitride (AlN) is one broadly used piezoelectric material for acoustic devices due to its high acoustic velocity, high thermal conductivity, excellent stability at high temperatures, and CMOS compatibility [2]–[4]. However, AlN's moderate electromechanical coupling (k^2) limits its performance at higher frequencies making it less suitable for certain high-frequency applications [5], [6]. It limits the achievable filter bandwidth (BW) and applicable frequency range [7]. Lately, scandium aluminum nitride (ScAlN) has gained attention in recent years for its potential applications in acoustic devices due to the enhanced piezoelectricity brought by Sc doping [8]–[10]. ScAlN has a higher piezoelectric coupling coefficient than AlN, which makes it more efficient at converting electrical signals into mechanical vibrations and vice versa [11], [12]. This property is important for the design of efficient and high-performance acoustic devices [13], [14]. In addition, ScAlN properties can be tuned by adjusting the doping concentration and crystal structure, which can allow for the design of customized acoustic devices [15], [16]. ScAlN also has a high acoustic velocity, which is similar to pure AlN, making it suitable for high-frequency applications [17]. Besides this, ScAlN has good thermal stability, which allows it to be operated at high temperatures without significant degradation [18]. This property is essential for many high-temperature applications in various industries [19]. Thus, studying losses in ScAlN/AlN at GHz frequencies is an important topic [20], [21].

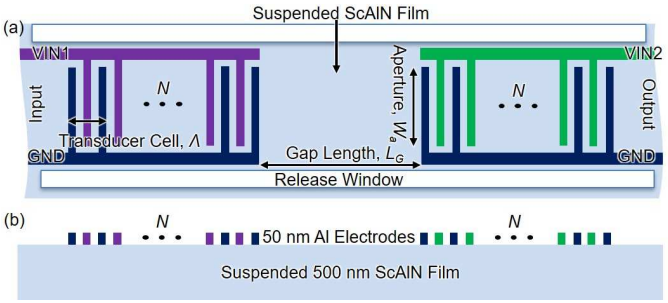

Fig. 1. (a) Top and (b) cross-sectional view schematic diagram of suspended thin-film ScAlN ADLs with key parameters.

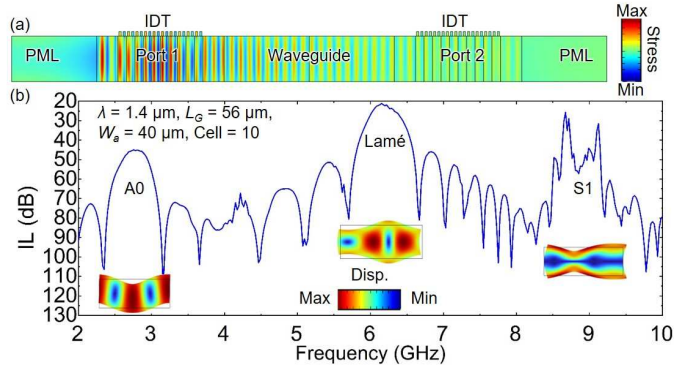

Fig. 2. (a) The ADL structure is simulated using COMSOL's FEA configuration, with the addition of Perfectly Matched Layers (PML) located at the edges of the ADL in order to avoid any reflections that could lead to unrealistic results. (b) COMSOL FEA simulated ADLs with λ of 1.4 µm, L_G of 56 µm, W_a of 40 µm, and N of 10. The inset displacement modes shape is plotted.

In the past, studies on the acoustic loss of piezoelectric thin films were conducted using theoretical calculations based on the properties of bulk materials, such as thermoelastic damping and phonon-phonon interaction [22]. However, because acoustic devices rely on thin-film structures, the properties of the material are often affected by non-ideal factors that arise during the deposition process. Therefore, these theoretical values mostly represent the upper limit in ideal situations. Recently, researchers have demonstrated thin-film piezoelectric resonators in AlN/ScAlN and lithium niobite ($LiNbO_3$) and conducted loss studies by comparing the maximum achievable Q at different frequencies [20]–[25]. However, there are other factors that contribute to loss, such as mechanical and electrical losses in the electrodes and anchors

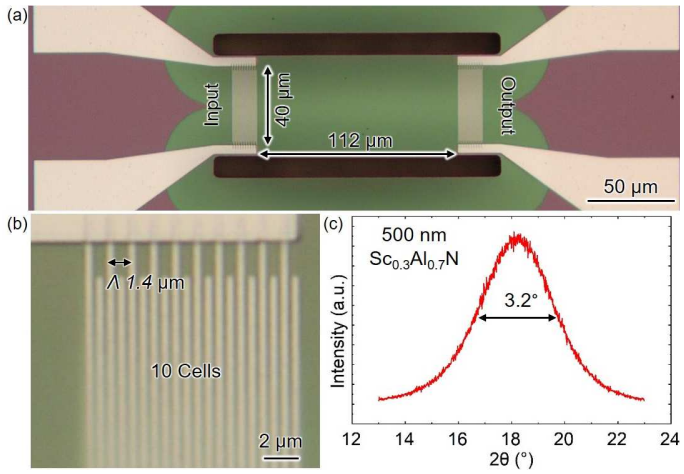

Fig. 3. (a) Zoom-out and (b) zoom-in optical images of the fabricated ADLs with λ of 1.4 µm, L_G of 112 µm. (c) XRD symmetric rocking curve of 500 nm thin-film ScAlN grown by PVD.

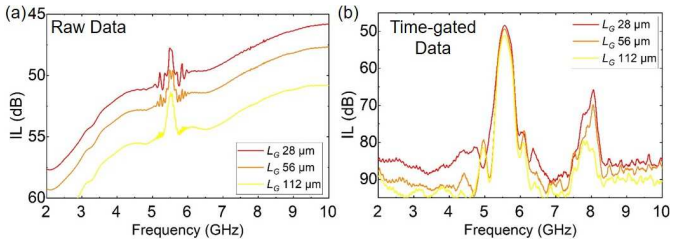

Fig. 4. (a) Measured raw transmission from the fabricated ADLs with λ of 1.4 µm and different L_G compared with (b) time-gated S21 data.

[29], [30]. These losses are intertwined with piezoelectric loss, so the Q of the resonator represents a lower limit for the overall loss. The actual limit of loss, which is determined by specific deposition methods, lies somewhere in between these two limits, but this has not yet been thoroughly investigated. Acoustic delay line (ADL) based loss studies, where traveling wave propagation loss is extracted from a group of ADLs with identical transducers but different waveguide lengths, has emerged as a promising alternative [31], [32]. However, most AlN/ScAlN ADLs are limited below 3 GHz due to transducer design and mode selection [9]. In this work, we describe the analysis of acoustic loss at higher-order Lamb waves with various order modes in thin-film ScAlN between 5 and 10 GHz.

II. Design & Simulation

The proposed ADLs schematic diagrams are suggested in Fig. 1 (a)-(b). Various patterned lateral wavelengths (λ) in 50 nm thick Al electrodes are fabricated on 500 nm thick ScAlN (30% Sc doping) sputtered on a silicon (Si) carrier wafer [33]. Fabricated suspended ScAlN waveguides are mechanically isolated from the surrounding thin film, through adjacent etch windows (defined by plasma ion-milling) and xenon difluoride (XeF_2) isotropic etching of the Si substrate [34], [35]. This structure supports a series of high-phase velocity modes in thin-film ScAlN and ensures energy confinement. Each λ unit cell utilizes λ/4 interdigitated transducers (IDT) with an aperture of 40 µm. Both input and output ports have 10 unit cells that face each other on opposite ends of the waveguide (spaced by gap length L_G). The IDT is linked to the probe pads with 100 µm

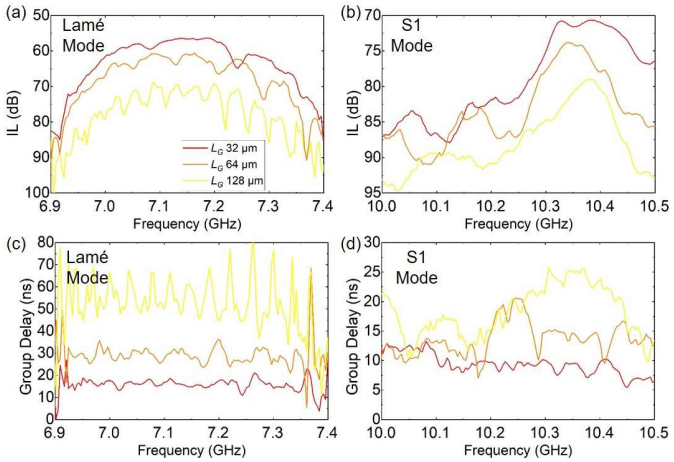

Fig. 5. Measured transmission of Lamé and S1 ADLs with λ of 0.8 µm and L_G between 32 µm and 128 µm showing (a)-(b) IL and (c)-(d) group delays.

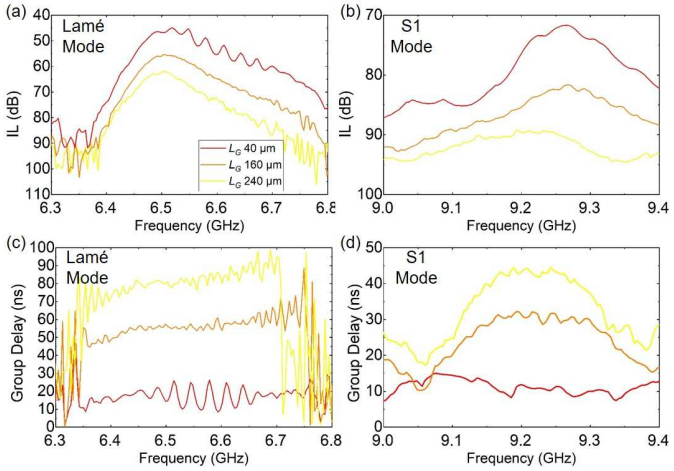

Fig. 6. Measured transmission of Lamé and S1 ADLs with λ of 1 µm and L_G between 40 µm and 240 µm showing (a)-(b) IL and (c)-(d) group delays.

spacing buslines. The proposed ADL design was simulated using COMSOL finite element analysis (FEA) to confirm the production and dissemination of higher-order Lamb tones (Fig. 2). To eliminate wave reflections and prevent standing waves in the model, perfectly matched layers (PML) are implemented at both ends of the model. The testbed has λ of 1.4 µm, L_G of 56 µm, W_a of 40 µm, and cell number N of transmission between the two ports generating three passbands, formed by three different modes. These include the fundamental antisymmetric (A0) Lamb, Lamé, and symmetric (S1) Lamb modes. Such higher-order operation enables extending loss study ADL testbeds beyond 5 GHz without relying on ultrafine IDTs.

III. Fabrication & Measurement

Optical images of the fabricated ADLs with λ of 1.4 µm, L_G of 112 µm are shown in Fig. 3 (a)-(b). The XRD rocking curve of the 500 nm sputtered ScAlN shows FWHM of 3.2° [Fig. 3 (c)] [36]. Four groups of ADLs with λ between 0.8 µm and 1.4 µm are implemented with gap length (L_G) from 20 µm to 240 µm, and measured with a Keysight P5027A network analyzer with -10 dBm power input in air.

The group with λ = 1.4 µm is first presented as the example. Measured data of ADLs with different L_G is first processed with a time-gate to remove EM feedthrough [comparison in Fig. 4

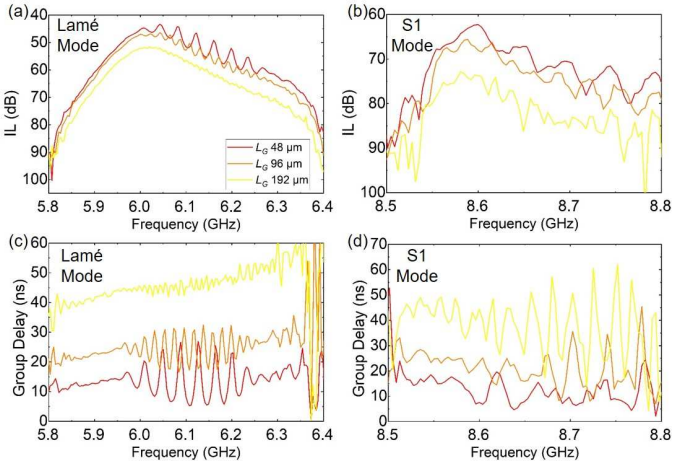

Fig. 7. Measured transmission of Lamé and S1 ADLs with λ of 1.2 µm and L_G between 48 µm and 192 µm showing (a)-(b) IL and (c)-(d) group delays.

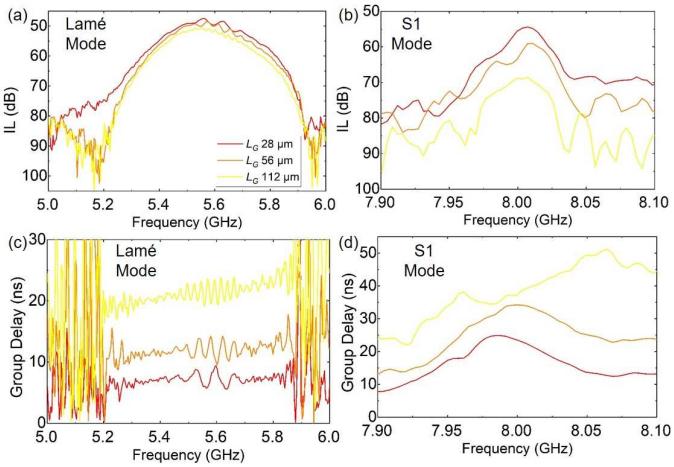

Fig. 8. Measured transmission of Lamé and S1 ADLs with λ of 1.4 µm and L_G between 28 µm and 112 µm showing (a)-(b) IL and (c)-(d) group delays.

(a)-(b)] [37]. Fig. 5 (a)-(d) depicts ADLs with a wavelength of 0.8 µm and a L_G range of 32 µm to 128 µm. The graphs show the insertion loss (IL) and group delay values for both Lamé and S1 modes, with the Lamé mode centered at 7.15 GHz and the S1 mode centered at 10.37 GHz. Fig. 6 (a)-(d) illustrate ADLs that have a wavelength (λ) of 1 µm and a L_G range of 40 µm to 240 µm. The graphs display the insertion loss (IL) and group delay values for both Lamé and S1 modes. The Lamé mode is centered at 6.5 GHz while the S1 mode is centered at 9.27 GHz. Fig. 7 (a)-(d) demonstrate ADLs with λ of 1.2 µm and L_G ranging from 48 µm to 192 µm. The graphs show insertion loss (IL) and group delay from Lamé and S1 modes, with the Lamé mode centered at 6.01 GHz and the S1 mode centered at 8.57 GHz. Next, ADLs with λ of 1.4 µm and L_G between 28 µm and 112 µm are presented in Fig. 8 (a)-(d), with insertion loss (IL) and group delay from Lamé and S1 plotted. Lamé and S1 modes are centered at 5.55 GHz and 8.02 GHz respectively. After utilizing a linear regression fitting as depicted in Fig. 9:

$$PL = PL_{dis} \cdot \frac{v_g}{f} \tag{1}$$

The propagation loss per unit length, measured in nepers per meter, is represented by PL_{dis}. The group velocity of the wave is measured in meters per second and is denoted by v_g, while the

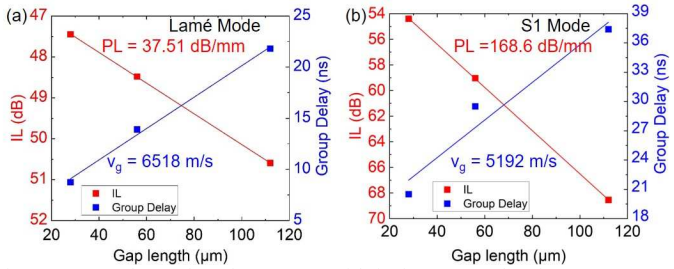

Fig. 9. Extracted v_g and PL from ADLs with λ of 1.4 µm and L_G between 28 µm and 112 µm at (a) Lamé mode and (b) S1 mode.

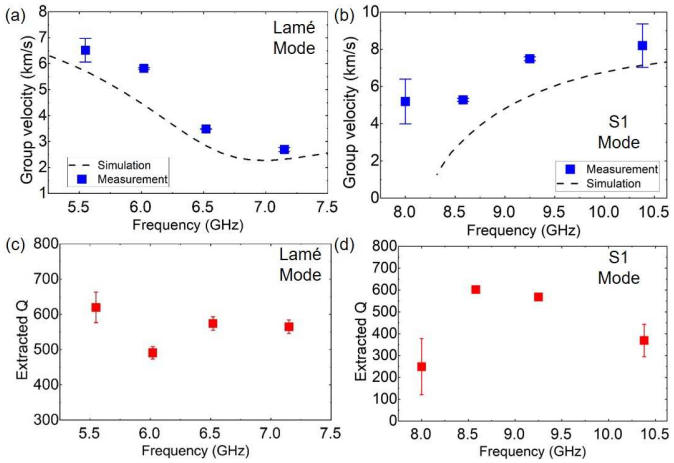

Fig. 10. Extracted and simulation v_g of (a) Lamé mode and (b) S1 mode in sputtered thin-film ScAlN. Extracted intrinsic Q of (c) Lamé mode and (d) S1 mode. The error bars are plotted.

operation frequency is measured in Hertz and represented by f. Using this information, the propagation Q is defined as:

$$Q = \frac{\pi}{PL} \tag{2}$$

Finally, the propagation characteristics of higher-order waves in suspended thin-film ScAlN are extracted in Fig. 9 (a)-(b). For Lamé mode at 5.55 GHz, propagation loss (PL) is 37.51 dB/mm and v_g is 6518 m/s. For the S1 mode at 8.02 GHz, PL is 168.6 dB/mm and v_g is 5192 m/s.

We also extended the analysis to a loss study between 5-10 GHz [Fig. 10 (a)-(d)]. The group velocity matches with the FEA, with the minor discrepancy caused by material property differences from theoretical values [38]. The sputtered 500 nm 30% doping ScAlN film shows Q around 500 for S1 and Lamé, while we suspect the limiting factor of the propagation loss is caused by the surface roughness.

IV. Conclusion

In this study, we presented a method for extracting acoustic losses in the frequency range of 5-10 GHz using specific groups of ADLs to measure the loss of higher-order lamb modes in thin-film ScAlN. The findings indicate that the propagation Q of higher-order Lamb modes is similar to or greater than that of lower-order modes. In order to enable future frequency scaling of microacoustic devices to the mm-wave band, a method to extract the inherent acoustic loss of piezoelectric thin films was also presented.

Acknowledgment

The authors thank the DARPA COFFEE program for funding support and Dr. Ben Griffin for helpful discussions.

REFERENCES

[1] I. L. Bajak, A. McNab, J. Richter, and C. D. Wilkinson, "Attenuation of acoustic waves in lithium niobate," *Journal of the Acoustical Society of America*, vol. 69, no. 3, 1981.

[2] Z. Schaffer, P. Simeoni, and G. Piazza, "33 GHz Overmoded Bulk Acoustic Resonator," *IEEE Microwave and Wireless Components Letters*, vol. 32, no. 6, 2022.

[3] T.-H. Hsu *et al.*, "An 8-inch commercial aluminum nitride MEMS platform for the co-existence of Lamb wave and film bulk acoustic wave resonators," *Journal of Micromechanics and Microengineering*, vol. 33, no. 5, 2023.

[4] A. Khandelwal *et al.*, "Self-Rolled-Up Aluminum Nitride-Based 3D Architectures Enabled by Record-High Differential Stress," *ACS Appl Mater Interfaces*, vol. 14, no. 25, 2022.

[5] C. Cassella, G. Chen, Z. Qian, G. Hummel, and M. Rinaldi, "RF passive components based on aluminum nitride cross-sectional lamé-mode MEMS resonators," *IEEE Trans Electron Devices*, vol. 64, no. 1, 2017.

[6] G. Piazza, M. Rinaldi, and C. Zuniga, "Nanoscaled piezoelectric aluminum nitride contour-mode resonant sensors," in *Proceedings of IEEE Sensors*, 2010.

[7] S. Link, R. Lu, S. Zhang, S. Gong, A. Dissanayake, and S. M. Bowers, "Enabling Channelizing Filters for High Impedance Nodes with Temperature Compensated Lamb-Wave Resonators," in *IFCS-ISAF 2020 - Joint Conference of the IEEE International Frequency Control Symposium and IEEE International Symposium on Applications of Ferroelectrics, Proceedings*, 2020.

[8] G. Giribaldi, L. Colombo, F. Bersano, C. Cassella, and M. Rinaldi, "Investigation on the Impact of Scandium-doping on the kt2 of ScxAl1-xN Cross-sectional Lamé Mode Resonators," in *IEEE International Ultrasonics Symposium, IUS*, 2020.

[9] R. Lu, S. Link, S. Zhang, M. Breen, and S. Gong, "Aluminum Nitride Lamb Wave Delay Lines with Sub-6 dB Insertion Loss," *Journal of Microelectromechanical Systems*, vol. 28, no. 4, pp. 569–571, Aug. 2019.

[10] R. Lu, S. Link, S. Zhang, M. Breen, and S. Gong, "Aluminum Nitride Lamb Wave Delay Lines with Sub-6 dB Insertion Loss," *Journal of Microelectromechanical Systems*, vol. 28, no. 4, 2019.

[11] Q. Wang, Y. Lu, S. Mishin, Y. Oshmyansky, and D. A. Horsley, "Design, Fabrication, and Characterization of Scandium Aluminum Nitride-Based Piezoelectric Micromachined Ultrasonic Transducers," *Journal of Microelectromechanical Systems*, vol. 26, no. 5, 2017.

[12] Y. Kusano, G. L. Luo, D. Horsley, I. T. Ishii, and A. Teshigahara, "36% Scandium-Doped Aluminum Nitride Piezoelectric Micromachined Ultrasonic Transducers," in *IEEE International Ultrasonics Symposium, IUS*, 2018.

[13] Y. Shimizu and T. Yanagitani, "Fabrication of high kt2and k' 352Sc0.4A10.6N thin films by RF magnetron sputtering," in *IEEE International Ultrasonics Symposium, IUS*, 2022.

[14] M. Park, Z. Hao, R. Dargis, A. Clark, and A. Ansari, "Epitaxial Aluminum Scandium Nitride Super High Frequency Acoustic Resonators," *Journal of Microelectromechanical Systems*, vol. 29, no. 4, 2020.

[15] R. Beaucejour et al., "Controlling Residual Stress and Suppression of Anomalous Grains in Aluminum Scandium Nitride Films Grown Directly on Silicon," *Journal of Microelectromechanical Systems*, vol. 31, no. 4, 2022.

[16] G. Piazza, V. Felmetsger, P. Muralt, R. H. Olsson, and R. Ruby, "Piezoelectric aluminum nitride thin fi lms for microelectromechanical systems," *MRS Bulletin*, vol. 37, no. 11. 2012. doi: 10.1557/mrs.2012.268.

[17] L. Colombo, et al., "Investigation of 20% scandium-doped aluminum nitride films for MEMS laterally vibrating resonators," in *IEEE International Ultrasonics Symposium, IUS*, 2017.

[18] Y. Song *et al.*, "Thermal Conductivity of Aluminum Scandium Nitride for 5G Mobile Applications and beyond," *ACS Appl Mater Interfaces*, vol. 13, no. 16, 2021.

[19] T. Mikolajick *et al.*, "Next generation ferroelectric materials for semiconductor process integration and their applications," *J Appl Phys*, vol. 129, no. 10, 2021.

[20] Z. Schaffer and G. Piazza, "Investigation of Damping and Ladder Filter Synthesis for 3 GHz 20% Scandium-Doped Aluminum Nitride Cross-Sectional Lame Mode Resonators," in *IEEE International Ultrasonics Symposium, IUS*, 2020.

[21] S. Rassay, D. Mo, and R. Tabrizian, "Dual-Mode Scandium-Aluminum Nitride Lamb-Wave Resonators Using Reconfigurable Periodic Poling," *Micromachines (Basel)*, vol. 13, no. 7, 2022.

[22] G. Vigevani, D. R. Myers, and A. P. Pisano, "PIEZO THERMOELASTIC MODEL FOR QUALITY FACTOR OPTIMIZATION OF RESONANT RINGS." [Online]. Available: http://asmedigitalcollection.asme.org/IMECE/proceedings-pdf/IMECE2010/44472/255/2708948/255_1.pdf

[23] A. Gao, R. Lu, and S. Gong, "Mitigation of AO spurious modes in AlN MEMS resonators with SiO2 addendums," in *2016 IEEE International Frequency Control Symposium, IFCS 2016 - Proceedings*, 2016.

[24] A. Bogner *et al.*, "Enhanced Piezoelectric AL1-XSCXN RF-MEMS Resonators for Sub-6 GHz RF-Filter Applications: Design, Fabrication and Characterization," in *Proceedings of the IEEE International Conference on Micro Electro Mechanical Systems (MEMS)*, 2020.

[25] M. Pirro, X. Zhao, B. Herrera, P. Simeoni, and M. Rinaldi, "Effect of Substrate-RF on Sub-200 nm Al0.7Sc0.3N Thin Films," *Micromachines (Basel)*, vol. 13, no. 6, 2022.

[26] M. Park, Z. Hao, D. G. Kim, A. Clark, R. Dargis, and A. Ansari, "A 10 GHz Single-Crystalline Scandium-Doped Aluminum Nitride Lamb-Wave Resonator," in *2019 20th International Conference on Solid-State Sensors, Actuators and Microsystems and Eurosensors XXXIII, TRANSDUCERS 2019 and EUROSENSORS XXXIII*, 2019.

[27] Y. Yang, L. Gao, and S. Gong, "Surface-Acoustic-Wave Devices Based on Lithium Niobate and Amorphous Silicon Thin Films on a Silicon Substrate," *IEEE Trans Microw Theory Tech*, vol. 70, no. 11, 2022.

[28] J. Kramer *et al.*, "57 GHz Acoustic Resonator with k2 of 7.3 % and Q of 56 in Thin-Film Lithium Niobate," in *2022 International Electron Devices Meeting (IEDM)*, 2022, pp. 16.4.1-16.4.4.

[29] G. Esteves *et al.*, "Al0.68Sc0.32N Lamb wave resonators with electromechanical coupling coefficients near 10.28%," *Appl Phys Lett*, vol. 118, no. 17, 2021.

[30] Y. Yang, L. Gao, R. Lu, and S. Gong, "Lateral Spurious Mode Suppression in Lithium Niobate A1 Resonators," *IEEE Trans Ultrason Ferroelectr Freq Control*, vol. 68, no. 5, 2021.

[31] S. Cho, Y. Wang, J. Kramer, K. Nguyen, and R. Lu, "Acoustic Delay Lines in Thin-Film Lithium Niobate on Silicon Carbide," in *2022 IEEE/MTT-S International Microwave Symposium - IMS 2022*, 2022, pp. 809–812.

[32] C. C. Yeh et al., "Sub-3 DB Insertion Loss Broadband Acoustic Delay Lines and High Fom Resonators in LiNbO3/SiO2/Si Functional Substrate," in *Proceedings of the IEEE International Conference on Micro Electro Mechanical Systems (MEMS)*, 2023.

[33] M. Pirro, B. Herrera, M. Assylbekova, G. Giribaldi, L. Colombo, and M. Rinaldi, "Characterization of Dielectric and Piezoelectric Properties of Ferroelectric AlScN Thin Films," in *Proceedings of the IEEE International Conference on Micro Electro Mechanical Systems (MEMS)*, 2021.

[34] S. Gong, R. Lu, Y. Yang, L. Gao, and A. E. Hassanien, "Microwave Acoustic Devices: Recent Advances and Outlook," *IEEE Journal of Microwaves*, vol. 1, no. 2, 2021.

[35] V. Chulukhadze *et al.*, "Frequency Scaling Millimeter Wave Acoustic Resonators using Ion Beam Trimmed Lithium Niobate," in *IFCS-EFTF 2023, Proceedings*, 2023.

[36] S. Rassay, F. Hakim, C. Li, C. Forgey, N. Choudhary, and R. Tabrizian, "A Segmented-Target Sputtering Process for Growth of Sub-50 nm Ferroelectric Scandium–Aluminum–Nitride Films with Composition and Stress Tuning," *Physica Status Solidi - Rapid Research Letters*, vol. 15, no. 5, 2021.

[37] J. Kramer et al., "Extracting Acoustic Loss of High-Order Lamb Modes at Millimeter-Wave Using Acoustic Delay Lines," in *International Microwave Symposium 2023 (submitted)*, 2023.

[38] S. H. Lee et al., "Influence of electrode configurations on the quality factor and piezoelectric coupling constant of solidly mounted bulk acoustic wave resonators," *J Appl Phys*, vol. 92, no. 7, 2002.